JOURNAL OF MATERIALS SCIENCE **38** (2003) 323–330

Microstructure and grain boundary microanalysis of X70 pipeline steel

J. WANG
The State Key Laboratory of Corrosion Science, Institute of Metal Research, The Chinese Academy of Sciences, Shenyang 110015, People's Republic of China

A. ATRENS
Division of Materials, The University of Queensland (UQ), Brisbane QLD 4072, Australia
E-mail: atrens@minmet.uq.oz.au

Grain boundaries (GBs), particularly ferrite: ferrite GBs, of X70 pipeline steel were characterized using analytical electron microscopy (AEM) in order to understand its intergranular stress corrosion cracking (IGSCC) mechanism(s). The microstructure consisted of ferrite (α), carbides at ferrite GBs, some pearlite and some small precipitates inside the ferrite grains. The precipitates containing Ti, Nb, V and N were identified as complex carbo-nitrides and designated as (Ti, Nb, V)(C, N). The GB carbides occurred (1) as carbides along ferrite GBs, (2) at triple points, and (3) at triple points and extending along the three ferrite GBs. The GB carbides were Mn rich, were sometimes also Si rich, contained no micro-alloying elements (Ti, Nb, V) and also contained no N. It was not possible to measure the GB carbon concentration due to surface hydrocarbon contamination despite plasma cleaning and glove bag transfer from the plasma cleaner to the electron microscope. Furthermore, there may not be enough X-ray signal from the small amount of carbon at the GBs to enable measurement using AEM. However, the microstructure does indicate that carbon does segregate to $\alpha:\alpha$ GBs during microstructure development. This is particularly significant in relation to the strong evidence in the literature linking the segregation of carbon at GBs to IGSCC. It was possible to measure all other elements of interest. There was no segregation at $\alpha:\alpha$ GBs, in particular no S, P and N, and also no segregation of the micro-alloying elements, Ti, Nb and V.

1. Introduction

Intergranular stress corrosion cracking (IGSCC) has been a significant (service) problem for gas pipelines. A particular example is the pipeline rupture caused by SCC of the main pipeline delivering gas to Sydney from the gas fields in central Australia. At that time, that pipeline provided the only natural gas supply to Sydney. That rupture was in an isolated part of Australia so there was little collateral damage from the resultant explosion and (1 km high) fire. The possible consequences are evident from the damage caused by a similar rupture of the Trans Canada Pipeline on 15 April 1996, 10 km south west of Winnipeg. That incident was also in an isolated area. The explosion and fireball resulted in the loss of one house, which was 178 m south of the rupture site.

Commonly, the mechanism of IGSCC of pipeline steels has been attributed to the segregation at $\alpha:\alpha$ Grain Boundaries (GBs) of S, P, N and C [1–15]. The evidence linking segregation of carbon at GBs to IGSCC is particularly strong [9–15]. For example, removal of carbon by wet hydrogen decarburization has been shown to stop IGSCC in steels [9, 11]. Long and Uhlig [12] showed that there was no IGSCC below a carbon concentration of about 0.002 wt% for very low carbon steels. Furthermore, the addition of carbon to pure iron has been shown to induce IGSCC [14, 15]. Parkins [1] states that the experimental results (particularly [16, 17]) are consistent with the iron carbide, and probably C in interstitial solution at the GB, acting as efficient points for cathodic discharge, facilitating the dissolution of the adjacent ferrite.

Our research at UQ seeks to understand the IGSCC of pipeline steels, with the particular aim to characterise the grain boundary composition using analytical microscopy (AEM) (with particular emphasis on S, P, N and C) and relate to the intergranular crack path during service SCC.

Our research has characterized the microstructures, the grain boundaries (GBs) and interphase boundaries (IBs) of the pipeline steels X42, X52 and X65 [18–21] using the best analytical electron microscopes available in Australia: the VG HB601 at the University Sydney, and the JEOL 2010 FEG AEM at ANSTO (the Australian Nuclear Science and Technology Organisation). It was not possible to measure carbon

at the GBs because of the inevitable surface hydrocarbon contamination [22]. It was possible to measure all other elements of interest. In contrast to the literature expectation that S or P segregate at GBs boundaries, there was no detectable segregation of P and S at GBs, so S and P are not likely to be responsible for IGSCC. This finding of no segregation of S and P has been substantiated by Danielson *et al*. [23]. Danielson *et al*. [23] also reported that the XPS (X-Ray Photo-Electron Spectroscopy) measurement technique was not appropriate to the measurement of GB composition of pipeline steels.

In contrast to the absence of segregation at $\alpha:\alpha$ GBs, Mn did segregate at the proeutectoid ferrite and pearlite IBs of X52 and X65. However, the Mn segregation is unlikely to be involved in IGSCC. The pattern of Mn segregation could be explained in terms of diffusion in the process zone ahead of the pearlite during the austenite to pearlite transformation and diffusion in the IBs between the proeutectoid ferrite and pearlite.

Higher strength, modern pipeline steels like X70 and X80 are becoming increasingly used in high pressure gas pipelines. These steels are cleaner (i.e., have lower S and P contents), are much lower in carbon to be nearly free of pearlite, and make use of micro-alloying additions such as Ti, Nb and V. It is expected that there would be a lower level of S and P at GBs but there is the possibility that some of the micro-alloying constitutes could segregate [23]. In order to understand the mechanism of SCC of these steels, it is necessary to study their microchemistry and microstructure, particularly their GBs. The present work has characterized the microstructure and the GBs of one particular X70 steel using analytical electron microscopy (AEM). Furthermore, particular attention was devoted to specimen preparation, cleaning and transfer to the AEM in order to try to produce a specimen free of surface hydrocarbon contamination, in order to measure carbon at GBs.

2. Experimental

2.1. Sample preparation

The X70 steel had the following chemical composition: 0.06% C, 0.007% N, 1.5% Mn, 0.24% Si, 0.008% S, 0.015% P, 0.13% Mo, <0.01% V, 0.06% Nb, 0.02% Ti, 0.036% Al, 0.01% Ni, 0.01% Cr. A piece of X70 steel pipe was cut from a service pipe and sliced using a slow speed saw into slices about 1 mm thick. These thin slices were stuck onto a flat holder using super glue and mechanically polished down to about 200 μm thickness. Polishing was done on both sides and from 120 to 1200 grit using silicon papers. Three-millimetre steel discs were punched from the thin slices and ground using a Gatan disc grinder until their thickness was around 40 μm. The 3 mm discs were jet-polished to produce AEM samples using a solution of 92% acetic acid and 8% perchloride acid at 30 V and 15°C. AEM samples were stored in reagent grade methanol between preparation and AEM characterization in order to minimize sample deterioration.

2.2. AEM sample cleaning and transfer

The AEM samples were plasma cleaned using the Fischione 1400 Plasma Cleaner in a gas mixture of 25% oxygen and 75% argon for 15 min. The theory of plasma cleaning is that free electrons are accelerated to high velocities by the oscillating electromagnetic field that excites the gas atoms and creates the plasma. The impinging plasma impacts the surface with energies of less than 20 eV. Cleaning is effected by the formation of reactive gas compounds, particularly oxygen ions, that react with carbonaceous material on the specimen and the specimen holder. The reaction products, carbon dioxide and water vapour, are removed by the vacuum system of the plasma cleaner.

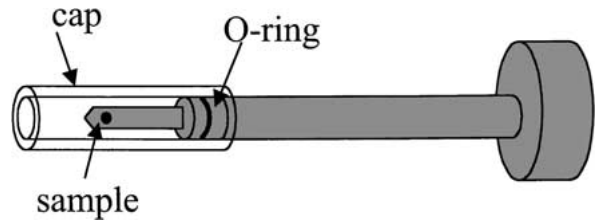

Figure 1 AEM sample holder and its cap.

The specimen was transferred from the plasma cleaner to the AEM using a glove bag transfer procedure in order to avoid exposure of the sample to laboratory air and the inevitable carbon contamination inherent in laboratory air [22]. A glove bag was sealed to the outside of the plasma cleaner sample chamber. The glove bag was flushed with pure argon in order to reduce the lab air residue inside the bag. The glove bag was filled with argon and then the gas was pumped out; then filled with argon and the mixture pumped out again. This process was repeated more than 10 times to reduce the air (and hydrocarbon) residue inside the glove bag. After plasma cleaning, the sample holder was taken out of plasma cleaner and capped with a plastic cap which sealed with the sample holder, as shown in Fig. 1. The glove bag was sealed to the Tecnai AEM sample chamber. The glove bag was again flushed with pure argon again over ten times, the cap of the sample holder was removed and the sample holder was quickly inserted into the Tecnai.

2.3. Microstructure and microanalysis of X70

The Philips Tecnai 20 is a field-emission-gun, high-resolution, analytical electron microscope equipped with energy dispersive X-ray spectroscopy (EDX). The GBs and precipitates were analysed using EDX with a probe size of about 1 nm. The microstructure was observed using the Tecnai 20 AEM in STEM mode.

3. Results

3.1. Microstructure of X70

The microstructure is shown in Fig. 2. There was a large amount of ferrite (α) and some GB carbides. The ferrite grain size, less than 5 μm, was smaller than for X42, X52 and X65. Typical ferritic GBs are shown in Fig. 2. Mostly, the ferrite GBs were curved. The carbon content in X70 is low, so there are few pearlite grains. The only one found in the thin area, shown in Fig. 3, was not very regular. The location of the GB carbides is shown in Fig. 4; the carbides were located (a) at ferrite GBs

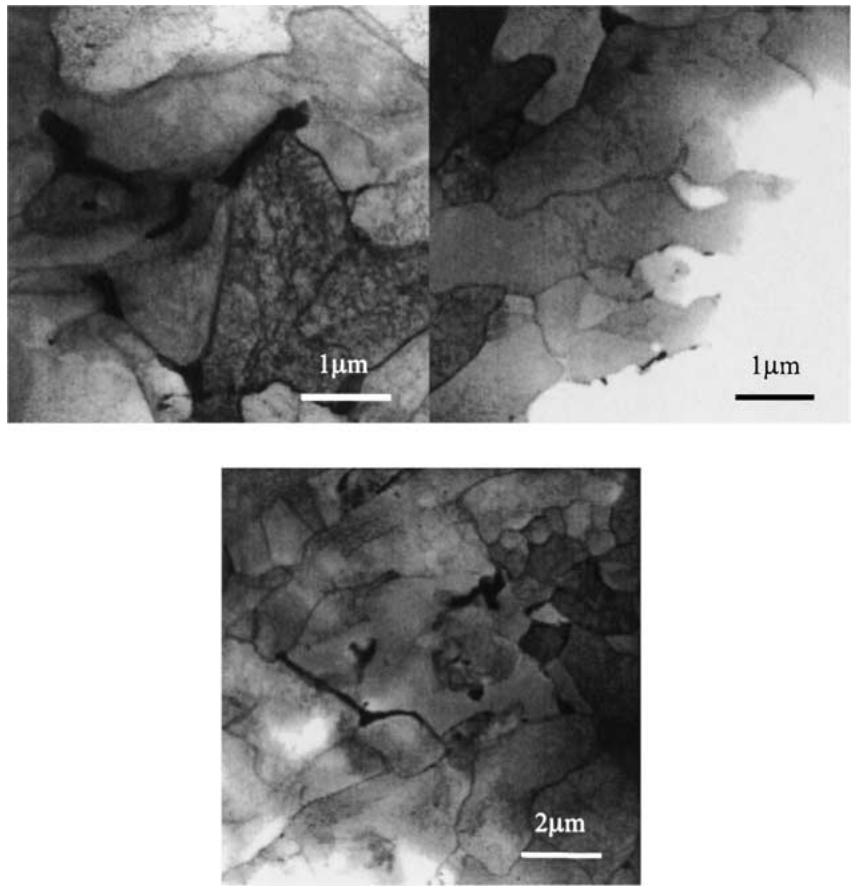

Figure 2 X70 microstructure observed in STEM mode.

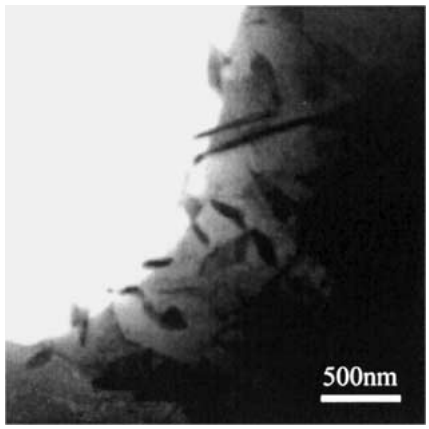

Figure 3 Pearlite grain of X70 observed in STEM mode.

along the whole GB, (b) at triple points, (c) extended from the triple point along the three ferrite GBs, and (d) at ferrite GBs as isolated GB carbides.

The high magnification views, as in Figs 5 to 7, show that there were fine particles inside ferrite grains. The particles were normally about 100 nm. Some were longer than 200 nm. EDX analysis showed that most of these particles, such as those illustrated in Fig. 5, contained Ti, Nb, V, N and C, as illustrated in Fig. 8. This is identified as a complex (Ti, Nb,V) carbonitride which may be designated as (Ti, Nb, V)(C, N). The carbides in Fig. 6 had essentially the same composition as those those in Figs 1–4 and contained both Fe and Mn but no Ti, Nb, V or N. Some ferrite grains had a high dislocation density as shown in Fig. 7.

3.2. Carbon analysis

Typical EDX spectra, as shown in Fig. 9, indicated a significant amount of carbon. The apparent carbon was almost 30 wt%. This means that there was sample surface hydrocarbon contamination despite all practical steps taken to produce a clean surface and prevent surface contamination.

3.3. Microanalysis of X70

The GBs of X70 were characterised by EDX using the Tecnai 20 AEM. The prior work on X42, X52 and X65 measured no GB segregation, particularly, no segregation of S and P at $\alpha:\alpha$ GBs, contrary to literature expectations. A typical EDX GB spectrum of X70, as shown in Fig. 9, indicated there was no S and P segregation at the $\alpha:\alpha$ GBs. This was similar to the result for X42, X52 and X65. Furthermore, there was no segregation of the micro-alloying constituents (Ti, Nb and V) at this kind of GB. Nor was there any appreciable segregation of N.

Figs 10 and 11 show a series of micro-analyses across an $\alpha:\alpha$ GB containing a GB carbide and Fig. 12 shows a typical spectrum from a GB carbide. These micro-analysis traces are typical of those measured. These showed that the grain boundary carbides were Mn rich, and in some cases were Si rich. The observation that the GB carbides contained more Mn than the ferrite was consistent with the previous work on X42, X52 and X65. These carbides contained no appreciable Ti, Nb, V or N as is clear from a typical spectrum as shown in Fig. 12.

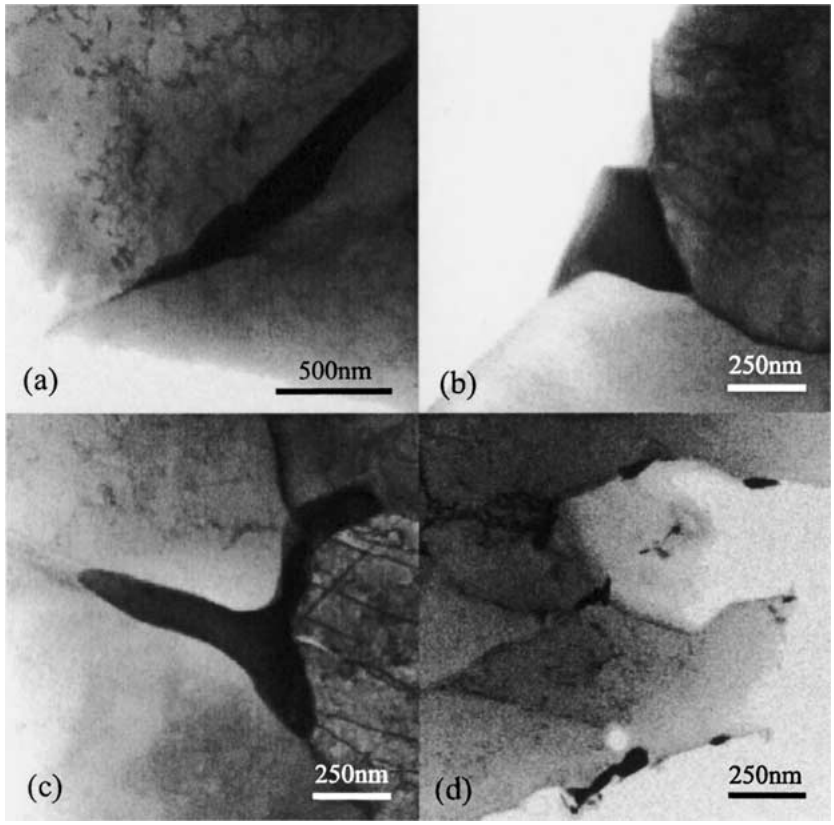

Figure 4 Typical ferrite grain boundary carbides of X70 observed in STEM mode. (a) At ferrite GBs along the whole GB, (b) at a triple point, (c) extended from the triple point along the three ferrite GBs, and (d) at ferrite GBs as isolated GB carbides.

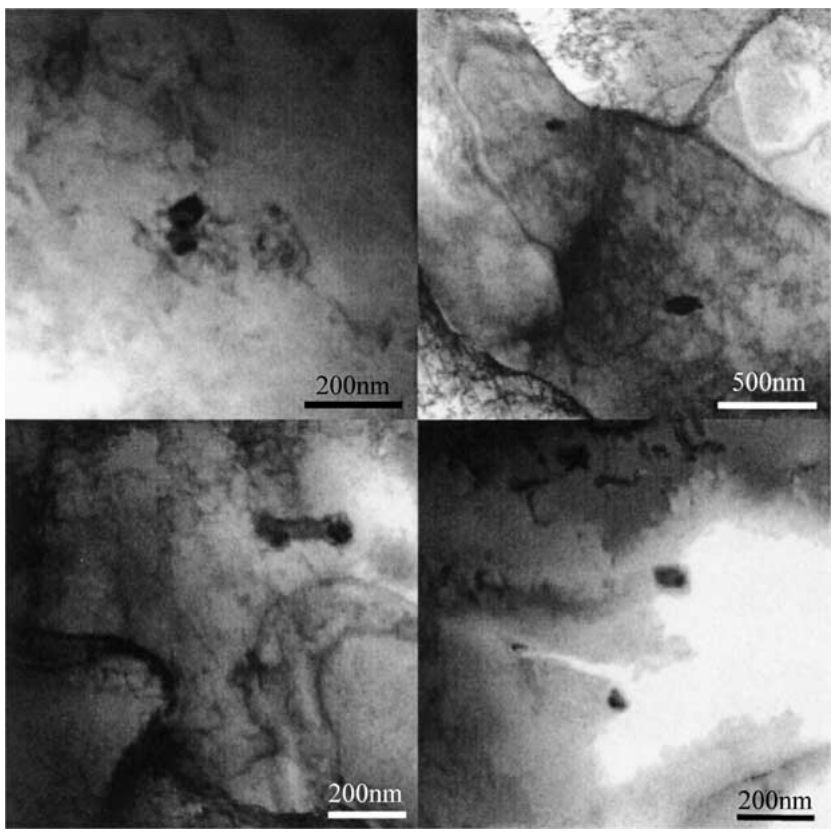

Figure 5 Fine precipitates inside ferrite grains containing Ti, Nb, V, C and N.

4. Discussion

4.1. Carbon contamination

The carbon micro-analysis measurement of the GB concentration of a steel sample seems impossible using AEM due to what appears to be inevitable carbon contamination when using specimen preparation and transfer procedures available to us in Australia because there are no transfer facilities in ultra-high vacuum.

Sample preparation methods used to-date include ion-beam thinning (used for [18]), jet-polishing (used

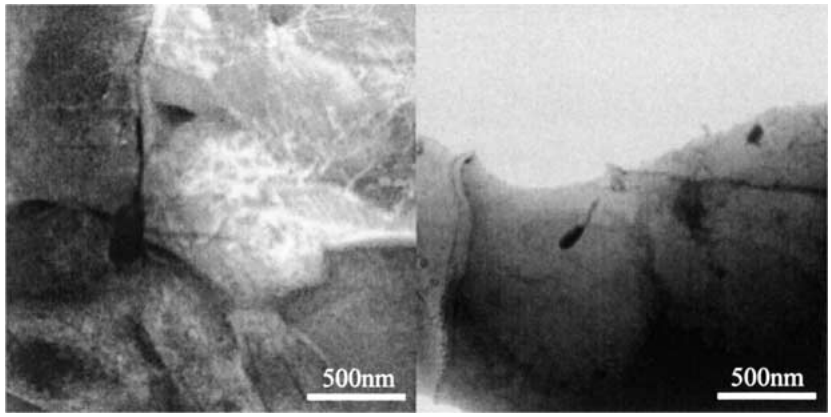

Figure 6 Fine precipitates consisting of Mn and Fe.

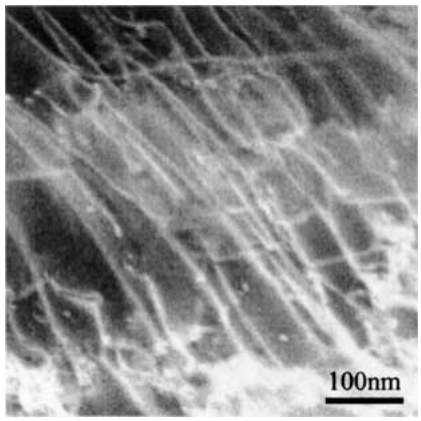

Figure 7 A ferrite grain with high dislocation density.

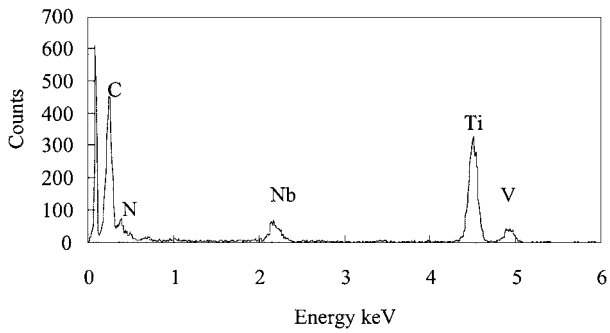

Figure 8 Typical EDX spectrum from a (Ti, Nb, V) (C, N) particle.

for [21]), and microtoming. During ion beam thinning, the sample is bombarded by an argon ion beam. The sample accumulates a surface film which consists of the diffusion pump oil, chamber redeposited ions, and amorphisation. It is possible that this kind of redeposit film can not be cleaned by plasma cleaning which is useful for removing absorbed hydrocarbons. For jet-polishing, on the sample surface, there is an anodic dissolution film which helps to brighten and smooth the surface. Plasma cleaning may have difficulty cleaning away this kind of film. On the other hand, the bath residue, which may not be washed out, also builds up the surface film.

The sample was stored in reagent grade methanol between preparation and analysis to prevent corrosion in air. The methanol is reported to have pH 5, but our measurement indicate pH 7 or pH 6.5. It is supposed that methanol does not corrode pipeline steels, and previous TEM observation showed that there was no corrosion

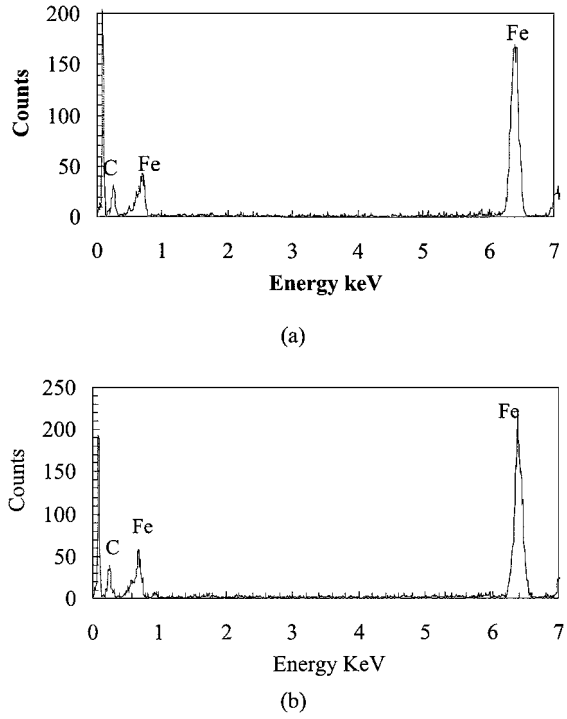

Figure 9 Typical EDX spectrum at a ferrite GB and inside a grain of X70. (a) At GB. (b) Inside a grain.

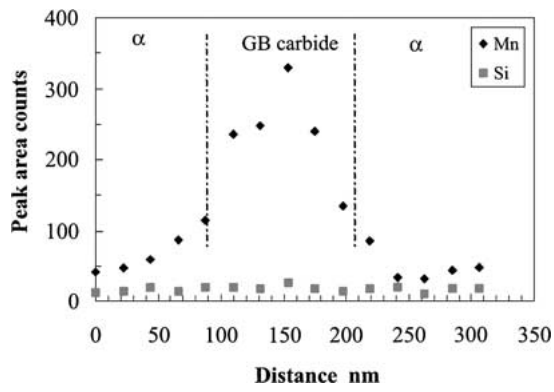

Figure 10 Mn and Si profile across a ferrite GB carbide.

around the thin area. Methanol is a hydrocarbon and it is likely to be cleaned away by the plasma cleaning.

Sample transfer is the most likely operation during which hydrocarbon contamination occurs. There are several chances for a sample to be exposed to (hydrocarbon containing) laboratory air. For jet-polishing, exposure to laboratory air occurred when the sample was

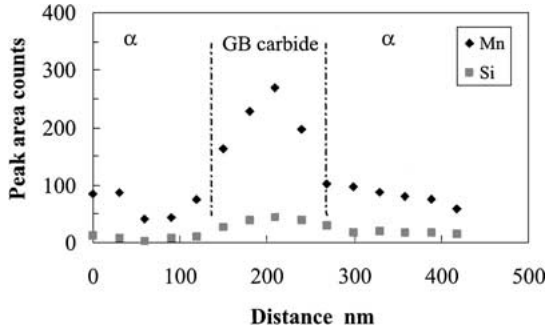

Figure 11 Mn and Si profile across a ferrite GB carbide.

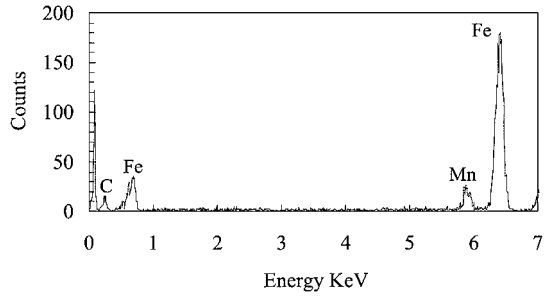

Figure 12 EDS spectrum from a ferrite GB carbide.

taken out of jet-polisher, washed several times with methanol step by step, and then put into storage in the methanol. All this processing was done in air. For ion beam thinning, when the sample thinning was finished, the sample should remain in the chamber during warming because water condenses on sample which was thinned in the cold stage. After being taken out of chamber, the sample is removed from the holder and then put into the methanol for storage. Before insertion into the AEM, the sample is taken out of the methanol, and put into the AEM sample holder in air. Then the sample holder was put into the plasma cleanser. The gas mixture of 75% argon and 25% oxygen was used in the plasma cleaning. Plasma is neutral overall but contains charged ions, electrons, molecules and gas. The charged ions, particularly oxygen ions, react with carbon and hydrogen to form carbon dioxide and water, which are removed by the vacuum pump. After plasma cleaning, the sample was transferred to the AEM using a glove bag transfer procedure in order to reduce the effect of exposure to laboratory air and the hydrocarbons inevitably contained therein [22].

The column inside the AEM is high vacuum. The sample stage is cooled by liquid nitrogen. The contamination from the AEM column is expected to be small.

The sample was not completely clean following the above processes. The surface film formed during sample preparation may contribute to the contamination and may be hard to clean away. If the plasma cleaning did remove all surface hydrocarbons, it still seems that there was some exposure to hydrocarbons, despite the precautions of the glove bag transfer.

4.2. EDX technique sensitivity

There is also the issue of the sensitivity of the EDX technique itself. During AEM operation [24], the incident electron beam ionises atoms in a truncated cone as

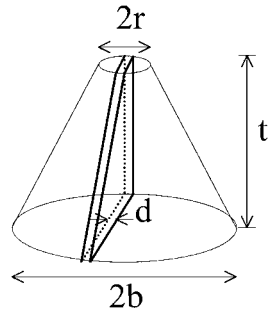

Figure 13 Excitation volume of the truncated cone.

illustrated in Fig. 13 [18, 22]. An ionised atom may lose energy by emitting a characteristic X-ray or it can emit an Auger electron. The probability of X-ray emission versus Auger emission is described by the fluorescence yield. The fluorescence yield is a strong function of the atom number Z, being proportional to Z^4. The fluorescence yield is $\sim 10^{-3}$ for carbon and is ~ 0.3 for Fe [24]. That means that, if the incident electrons ionise 1000 carbon atoms, only one characteristic X-ray is expected, whereas for 1000 Fe atoms ionised 300 characteristic X-rays are expected. This leads to the question, even if there is no consideration of carbon contamination and carbon X-ray absorption, can this amount of carbon be detectable?

If there is a sufficient X-ray signal, quantification of the X-ray signal typically relies of a calibration procedure. In this quantification it is possible to neglect the issue of the fluorescence yield [24]. However, for the case of carbon segregation at GBs, is there sufficient carbon X-ray signal above the background? If there are few carbon atoms at the GBs, the low fluorescence yield of X-rays from carbon atoms may mean that there is too little X-ray signal to detect. This may be estimated as follows [18, 22]. The excitation volume of the truncated cone from which X-rays may be detected is given by:

$$V_{\mathrm{EX}} = (\pi/3)\{r^2 + rb + b^2\}t \qquad (1)$$

where r is the electron beam radius as it enters the specimen, and b is exit beam radius at the exit side of the specimen (i.e., beam broadening in specimen thickness t). The volume of carbon, assuming the GB is covered with carbon to a thickness d, is given by

$$V_{\mathrm{GB}} = td(r + b) \qquad (2)$$

so that the weight fraction of carbon within the analysed volume is given by

$$F_{\mathrm{C}} = \rho_{\mathrm{C}} V_{\mathrm{GB}} / \{\rho_{\mathrm{Fe}}(V_{\mathrm{EX}} - V_{\mathrm{GB}}) + \rho_{\mathrm{C}} V_{\mathrm{GB}}\} \qquad (3)$$

where ρ_{C} is the density of carbon and ρ_{Fe} is the density of iron. Using the following values, $d = 0.1$ nm, $r = 0.5$ nm, $b = 5$ nm for a typical specimen of thickness 50 nm, $\rho_{\mathrm{C}} = 2.25$, and $\rho_{\mathrm{Fe}} = 7.88$, Equation 3 yields

$$F_{\mathrm{C}} = 0.0055 \qquad (4)$$

If the relative fluorescence yields for carbon and Fe are taken into account, the apparent weight fraction carbon is evaluated to be

$$F_{\mathrm{ap}} = 0.0055(10^{-3}/0.3) = 0.000018 \qquad (5)$$

This implies that it is necessary to be able to measure a carbon peak that is 1.8×10^{-5} smaller than the Fe peak. This appears to be problematical, considering the peak heights in the various spectra, i.e., in Figs 8, 9 and 12.

4.3. Microstructure development

The literature [25] indicates that X70 steel is produced by hot thermo-mechanical processing. The slab is reheated to 1250°C in order to ensure complete solution of the micro-alloying carbo-nitrides (Ti, Nb, V)(C, N). Rough rolling is completed above about 1030°C with the metallurgical objective of achieving the finest possible grain size. TiN particle control is used to inhibit the growth of the austenite grains. The finish rolling is commenced below the austenite non-recrystallization temperature. The prime intention is to accumulate rolling strain within the austenite grains so that on subsequent ferrite transformation, there are many ferrite nucleation sites and a very fine ferrite grain size results.

The microstructure, as observed in the present study, consisted of a large amount of ferrite (with a grain size less than 5 μm), some GB carbides and few pearlite grains. Some ferrite grains had a high dislocation density. The grain boundary carbides contained Fe, Mn and sometimes Si. They contained no Ti, Nb, V or N. The typical thickness of GB carbides was about 100 nm. This microstructure is consistent with the low carbon content of the X70 steel. There were some fine precipitates inside the ferrite grains which are attributed to complex mixed Ti, Nb and V carbo-nitrides which can be designated as (Ti, Nb, V)(C, N). These fine precipitates were the only microstructural features associated with the micro-alloying additions: Ti, Nb and V; and there was not two obvious populations of precipitates containing the micro-alloying.

The precipitates within the ferrite grains designated herein as (Ti, Nb, V)(C, N) and the high dislocation density within the ferrite grains reflect the thermo-mechanical treatment described above, which are associated with the hot working sequence at temperatures at which the steel is austenitic. Apart from their influence as described above, they do not seem to have had an influence in the further development of the microstructure and particularly the development of the ferrite grain boundaries.

The following mechanisms were important in the final development of the microstructure, particularly the ferrite grain boundaries. The composition of the steel is such that all the carbon (except for carbon associated with (Ti, Nb, V)(C, N)) is in solid solution in the austenite at high temperatures during processing, and that there is more carbon than can be accommodated in solid solution in the ferrite on cooling to room temperature. The steel has a low carbon content and contains little pearlite. This means that during cooling from the austenite, most of the austenite transforms to ferrite. During cooling below the A1 temperature, the maximum solubility of carbon in the ferrite lattice decreases, and the ferrite becomes supersaturated with carbon. The carbon accommodation in ferrite lattice is associated with lattice strain, because the carbon atom is larger than the available interstitial lattice sites. There is a driving force for the carbon atoms to diffuse to the GBs, which have a much more disordered structure and can more easily accommodate the carbon.

When the grain boundary carbon content becomes sufficiently large, iron carbide particles precipitate. These carbides grow by the accumulation of more carbon during further cooling.

Consequently, it is reasonable to expect that, if there is insufficient carbon available to form a GB carbide, then there remains the carbon segregation at the GB. Indeed, Fig. 2 indicates that there are many GBs with carbides and also many GBs with no carbides. It is these GBs with no carbides that might be particularly expected to contain segregated carbon. Furthermore, it is relatively easy to think of models that would produce preferential anodic dissolution if there was carbon segregation. Therefore it is important to characterise experimentally the carbon content of the grain boundaries of pipeline steel.

There are a number of theoretical expressions that relate to segregation at GBs [26, 27]. The most popular appears to be the Langmuir-McLean representation:

$$C_{\mathrm{GB}} = \theta/(1-\theta) = C_{\mathrm{B}} \exp(-\Delta G/RT) \qquad (6)$$

where C_{GB} is the GB concentration, θ is the GB coverage in monolayers, C_{B} is the bulk concentration, ΔG the Gibbs free energy associated with the segregation to the GB, R is the gas constant and T the absolute temperature. The ΔG associated with carbon in steels given by Faulkner *et al*. [28] is considerably larger than that for P indicating stronger segregation for carbon than for phosphorus. This corresponds to the enrichment factor in α-Fe of carbon $\alpha_{\mathrm{C}} \sim 10^4$ being considerably larger than for phosphorus $\alpha_P \sim 10^2$ [27, 28], where the enrichment factor, α, is given by

$$\alpha = C_{\mathrm{GB}}/C_{\mathrm{B}} \qquad (7)$$

A review of the literature did not reveal any measurements of GB carbon concentrations [29, 30] relating to pipeline steels. Of interest are the measurements in related systems of carbon segregation at (a) $\alpha : \alpha$ GBs in low carbon steels [31] and (b) at the prior γ GBs (which are within the ferrite) in steels e.g., [32].

4.4. Microanalysis

Typical EDX spectrum indicated a significant amount of carbon which is attributed to surface hydro-carbon contamination on the specimen surface. Plasma cleaning was carried out in order to remove the surface hydrocarbon contamination to enable the carbon microanalysis at the GBs. Moreover, after plasma cleaning, the sample was transferred to the AEM using a glove bag transfer procedure in order to reduce the effect of exposure to laboratory air and the hydrocarbons inevitably contained therein [22]. However, the EDX spectrum in Fig. 9 showed that the carbon peak was very obvious. This means that there was sample surface hydrocarbon contamination despite all practical steps taken to produce a clean surface and prevent surface contamination.

Our work to date thus leads us to the situation where experience indicates that the segregation of carbon to

$\alpha:\alpha$ GBs in pipeline steels is indirectly implicated in IGSCC, the microstructure leads to the inference that it is likely that there is carbon segregation to the $\alpha:\alpha$ GBs, there is a theoretical expectation of strong GB segregation of carbon in α-Fe, and there is evidence of carbon segregation in related systems. But available AEM techniques do not allow the measurement of GB carbon concentration, particularly because of surface hydocarbon contamination, due to exposure of the AEM specimen to laboratory air before insertion into the AEM.

The Tecnai 20 AEM allowed characterisation of the to $\alpha:\alpha$ GBs of X70 for all elements of interest, with this caveat regarding carbon. A typical EDX spectrum of X70, as shown in Fig. 9, indicated there was no S and P segregation at the $\alpha:\alpha$ GBs. This was similar to the result for X42, X52 and X65. Furthermore, there was no segregation of the micro-alloying constituents, Ti, Nb and V, at this kind of GB. There was also no N.

5. Conclusions

1. There is strong evidence in the literature linking the segregation of carbon at GBs to IGSCC.

2. It was not possible to measure the GB carbon concentration due to surface hydrocarbon contamination despite plasma cleaning and glove bag transfer from the plasma cleaner to the electron microscope. Furthermore, there may not be enough X-ray signal from the small amount of carbon at the GBs to enable measurement using AEM.

3. The microstructure of X70 steel was ferritic/pearlitic. It contained predominantly ferrite, GB carbides and some pearlite. Inside the ferrite grains there were small precipitates containing Ti, Nb, V and N that are attributed to complex carbo-nitrides designated as (Ti, Nb, V)(C, N).

4. The GB carbides occurred (1) as isolated carbides along ferrite GBs, (2) at triple points, and (3) at triple points and extending along the three ferrite GBs.

5. This microstructure indicates that carbon does segregate to $\alpha:\alpha$ GBs during microstructure development, and there is a theoretical basis for expecting carbon segregation at GBs.

6. The GB carbides were Mn rich, and sometimes also Si rich. They contained no micro-alloying elements: Ti, Nb, V. They also contained no N.

7. There was no measurable segregation at ferrite: ferrite GBs, in particular no S, P and N, and also no segregation of micro-alloying elements, Ti, Nb and V.

Acknowledgment

The work is funded by ARC SPIRT grant sponsored by Agility Team Build, OneSteel Oil and Gas Pipe and Woodside Energy Ltd. We also thank CMM in UQ for supporting the access of Tecnai 20, for the strong support of using Tecnai and glove bag transfer from Dr John Barry in CMM. The travel fee was partly supported by The Special Funds for the Major State Basic Research Projects G19990650, Institute of Metal Research, the Chinese Academy of Sciences.

References

1. R. N. PARKINS, *Corrosion* **52** (1996) 363.
2. *Idem*., in 5th Symposium on Line Pipe Research" (American Gas Association Inc, 1974) p. V, U1-40.
3. R. P. MAGDOWSKI and M. O. SPEIDEL, in Parkins Symposium on Fundamental Aspects of SCC, edited by S. M. Bruemer (TMS, 1992) p. 341.
4. K. L. MOLOZNIK, C. L. BRIANT and C. J. MCMAHON, *Corrosion* **35** (1979) 331.
5. M. P. SEAH, P. J. SPENCER and E. D. HONDROS, *Met. Sci.* **13** (1979) 307.
6. C. LEA, *ibid*. **14** (1980) 107.
7. E. D. HONDROS and M. P. SEAH, *Int. Met. Rev*. **22** (1977) 262.
8. C. LEAH and E. D. HONDROS, *Proc. Royal Soc*. **377A** (1981) 477.
9. R. N. PARKINS, *J. Iron and Steel Inst.* **172** (1952) 149.
10. L. M. LONG and H. H. UHLIG, *J. Electrochem, Soc*. **112** (1965) 964.
11. J. T. WABER and H. J. MCDONALD, "Stress Corrosion Cracking of Mild Steel" (Corrosion Publishing, Pittsburg, 1947).
12. V. A. PHILLIPS, *Acta Met*. **11** (1963) 139.
13. M. J. HUMPHRIES and R. N. PARKINS, in 4th International Congress Metallic Corrosion, Houston TX (NACE, 1969) p. 151.
14. E. BELHIMER, PhD thesis, University of Newcastle upon Tyne, 1987.
15. G. TRAUBER and H. J. GRABKE, *Corrosion Science* **19** (1979) 793.
16. J. FLIS, *Corros. Sci*. **25** (1985) 317.
17. M. HENTHORN and R. N. PARKINS, *Brit. Corros. J* **2** (1967) 186.
18. J. Q. WANG, A. ATRENS, D. R. COUSENS, P. M. KELLY, C. NOCKOLDS and S. BULCOCK, *Acta Mater*. **46** (1998) 5677.
19. J. Q. WANG, A. ATRENS, D. R. COUSENS, C. NOCKOLDS and S. BULCOCK, *J. Mater. Sci.* **34** (1999) 1711.
20. J. Q. WANG, A. ATRENS, D. R. COUSENS and N. N. KINAEV, *ibid*. **34** (1999) 1721.
21. J. Q. WANG, A. ATRENS and D. R. G. MITCHELL, in Corrosion 2001 (NACE International, Houston, TX) Paper 01210.
22. D. R. COUSENS, B. J. WOOD, J. Q. WANG and A. ATRENS, *Surface and Interface Analysis* **29** (2000) 23.
23. M. J. DANIELSON, R. H. JONES and P. DUSEK, in Corrosion 2001 (NACE International, Houston, TX) Paper 01212.
24. D. B. WILLIAMS and C. B. CARTER, "Transmission Electron Microscopy" (Plenum, New York, 1996).
25. J. G. WILLIAMS, C. R. KILLMORE, F. J. BARBARO, J. PIPER and L. FLETCHER, *Materials Forum* **20** (1996) 13.
26. C. L. BRIANT and H. J. GRABKE, *Materials Science Forum* **46** (1989) 253.
27. P. LEJCEK and S. HOFMANN, *Critical Reviews in Solid State and Materials Sciences* **20** (1995) 1.
28. E. D. HONDROS and M. P. SEAH, *Int. Met. Review* **22** (1977) 867.
29. M. THUVANDER and H. O. ANDREN, *Materials Characterisation* **44** (2000) 87.
30. H. O. ANDREN, *Micron* **32** (2001) 713.
31. B. MINTZ, H. KE and G. D. W. SMITH, *Mater. Sci. Technol*. **8** (1992) 537.
32. J. R. COWAN, H. E. EVANS, R. B. JONES and P. BOWEN, *Acta Mater*. **46** (1998) 6565.

Received 19 November 2001
and accepted 18 July 2002